

Resonant thermal energy transfer to magnons in a ferromagnetic nanolayer

Michal Kobecki^{1*}, Alexey V. Scherbakov^{1,2*}, Tetiana L. Linnik³, Serhii M. Kukhtaruk^{1,3}, Vitalyi E. Gusev⁴, Debi P. Pattnaik⁵, Ilya A. Akimov^{1,2}, Andrew W. Rushforth⁵, Andrey V. Akimov⁵, and Manfred Bayer^{1,2}

Energy harvesting is a modern concept which makes dissipated heat useful by transferring thermal energy to other excitations. Most of the existing principles for energy harvesting are realized in systems which are heated continuously, for example generating DC voltage in thermoelectric devices. Here we present the concept of high-frequency energy harvesting where the dissipated heat in a sample excites resonant magnons in a 5-nm thick ferromagnetic metal layer. The sample is excited by femtosecond laser pulses with a repetition rate of 10 GHz which results in temperature modulation at the same frequency with amplitude ~ 0.1 K. The alternating temperature excites magnons in the ferromagnetic nanolayer which are detected by measuring the net magnetization precession. When the magnon frequency is brought onto resonance with the optical excitation, a 12-fold increase of the amplitude of precession indicates efficient resonant heat transfer from the lattice to coherent magnons. The demonstrated principle may be used for energy harvesting in various nanodevices operating at GHz and sub-THz frequency ranges.

The transfer of thermal energy to mechanical, electrical or magnetic excitations is of great interest and is widely considered for energy harvesting when waste heat is transferred to more usable types of energy [1]. The rational utilization of heat is a critical task for nanoscale electronics, where operations are accompanied by extensive production of parasitic heat. Nanoscale devices for communication and computing operate with digital signals, which are generated by ultrafast current or optical pulses with high repetition rate. The heat generated in this case is also modulated at the same frequency and could be transferred to non-thermal types of excitation which become the elements of the energy harvesting process. This process would be most efficient in the case of resonance, when the modulated heat is transferred to a sub-system with the same intrinsic frequency. Resonant heat transfer is widely used in photo-acoustics and was proposed for the first time by Bell in 1881 [2]. There the modulated optical signal is absorbed in a system with acoustic resonance at the frequency of modulation and as a result the modulated heat resonantly excites the acoustic wave. Modulation frequencies in photo-acoustics do not exceed the MHz frequency range [3], while thermomodulation with frequencies up to 400 GHz [4] is used in picosecond ultrasonics for studying sub-THz coherent phonon dynamics.

Here we propose to convert high frequency (GHz) modulated heat to magnons, which are collective spin excitations in magnetically ordered materials. The manipulation of coherent high-frequency magnons on the nanoscale is one of the most prospective concepts for information technologies [5], also in the quantum regime [6]. While the most common way to excite coherent magnons is non-thermal and based on microwave techniques [7], thermal methods have proven successful in ferromagnetic metals. These methods are based on ultrafast modulation of the magnetic anisotropy induced by rapid lattice heating, e.g. due to the

¹Experimentelle Physik 2, Technische Universität Dortmund, Otto-Hahn-Str. 4a, 44227 Dortmund, Germany. ²Ioffe Institute, Politechnicheskaya 26, 194021 St. Petersburg, Russia. ³Department of Theoretical Physics, V.E. Lashkaryov Institute of Semiconductor Physics, Pr. Nauky 41, 03028 Kyiv, Ukraine. ⁴LAUM, CNRS UMR 6613, Le Mans Université, 72085 Le Mans, France. ⁵School of Physics and Astronomy, University of Nottingham, Nottingham NG7 2RD, United Kingdom.

*e-mail: michal.kobecki@tu-dortmund.de; alexey.shcherbakov@tu-dortmund.de.

absorption of optical pulses [8,9]. In ferromagnetic metals, the intrinsic magnon frequency depends on the external magnetic field and may be varied between ~ 1 and ~ 100 GHz [10]. This range covers the clocking frequency for most electronic devices and, thus, magnons are suitable to receive dissipated heat modulated at the resonant frequency.

In the present paper, we introduce the concept of transferring heat dissipated in a semiconductor from the relaxation of hot electrons excited by a 10-GHz laser to coherent magnons. In our experiments the energy harvester is a metallic ferromagnetic film of 5-nm thickness grown on a semiconductor substrate. We demonstrate an efficient heat–magnon transfer by measuring a 12-fold increase of the fundamental magnon mode amplitude at the resonance conditions. The experiments and related theoretical analysis show that GHz modulation of the temperature on the scale of ~ 0.1 K is sufficient for the excitation of magnons with amplitude reliable for the operation of spintronic devices.

Results

The ferromagnetic energy harvester is a 5-nm layer of Gallenol ($\text{Fe}_{0.81}\text{Ga}_{0.19}$) grown by magnetron sputtering on a (001) semi-insulating GaAs substrate and covered by a 2-nm Cr cap layer to prevent oxidation. The chosen composition of Fe and Ga is characterized by a high Curie temperature ($T_c \approx 900$ K) and large saturation magnetization M_0 [11]. Experiments were carried out at ambient conditions at room temperature with an external magnetic field, \mathbf{B} , applied in the layer plane at an angle $-\pi/8$ from the [100] crystallographic direction, which corresponds to the maximal sensitivity of the magnetization, \mathbf{M} , to the temperature-induced changes of the magnetic anisotropy [12]. In the studied layer the lowest, fundamental mode of the quantized magnon spectrum is well separated from the higher-order modes due to the large exchange mode splitting [12]. As a result, the magnon spectrum consists of a narrow single spectral line of Lorentzian shape with a width of ≈ 500 MHz. Examples of the magnon spectrum for several values of B measured by monitoring the magnetization precession excited by a single optical pulse are shown in Fig. 1a (for details see Methods section). The experimentally measured dependence of magnon frequency f on B is shown by the symbols in the right panel of Fig. 1a.

Fig. 1b illustrates a schematic of the pump-probe experiment for magnon energy harvesting from high-frequency modulated heat. A femtosecond pump laser with repetition rate $f_0 = 10$ GHz and average power up to $W = 150$ mW is used for modulation of the lattice temperature. A second laser with repetition rate of 1 GHz and average power of 18 mW is used to probe the response of the magnons to the high-frequency heat modulation by means of the transient polar Kerr rotation effect. The pump and probe beams are focused on the $\text{Fe}_{0.81}\text{Ga}_{0.19}$ layer into overlapping spots of $17 \mu\text{m}$ and $14 \mu\text{m}$ diameter, respectively, using different sectors of the same reflective microscope objective (for details see the Methods section).

Fig. 1c (upper panel) shows the calculated temporal evolution of the lattice temperature $T(t)$ in the $\text{Fe}_{0.81}\text{Ga}_{0.19}$ layer under 10-GHz pump optical excitation. The calculations were performed by solving the heat equations taking into account the thermal resistance at the $\text{Fe}_{0.81}\text{Ga}_{0.19}/\text{GaAs}$ interface (see Methods section and Supplementary Notes 1 and 2). The temperature modulation amplitude $\delta T \sim W/(Cr^2)$, where C and r are the heat capacity and radius of the excitation spot. It is seen that the lattice temperature oscillates with amplitude δT on a stationary background which exceeds the room temperature T_0 by ΔT . Both ΔT and δT increase linearly with W : $\delta T = pW$ and $\Delta T = PW$ where p and P are constants which for our structure equal to 4.9K/W and 510 K/W respectively. The temperature modulation is not

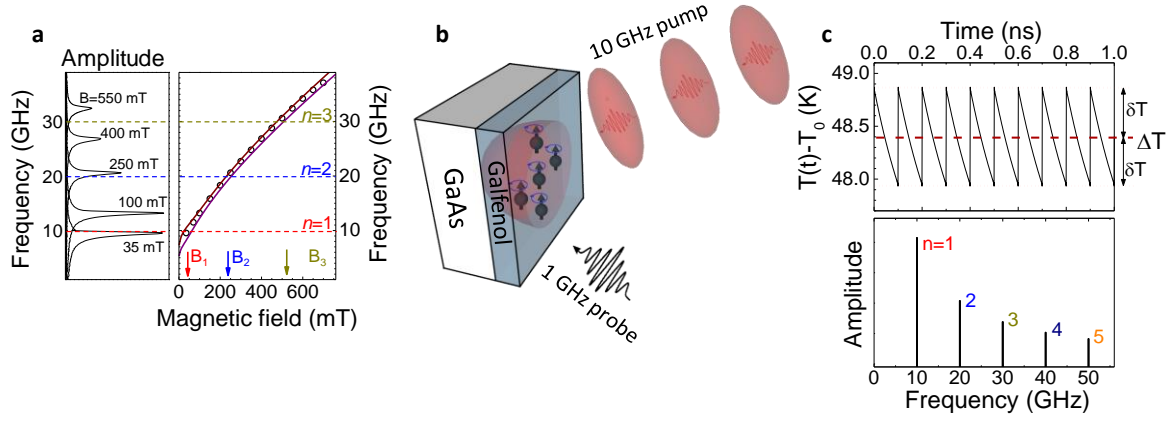


Figure 1. **a** Fast Fourier transform spectra showing the fundamental magnon mode for several values of magnetic field, B , (left panel) and the field dependence of its frequency, f , (right panel) for the 5-nm thick $\text{Fe}_{0.81}\text{Ga}_{0.19}$ energy harvesting layer. Symbols show $f(B)$ obtained by fast Fourier transformation of Kerr rotation signals measured in a single pulse pump-probe experiment. Solid lines are calculated dependences for $\Delta T=0$ K (upper curve) and $\Delta T=200$ K (lower curve). The dashed horizontal lines show the frequencies of the harmonics in the temperature modulation spectrum induced by the 10-GHz optical excitation. The vertical arrows indicate the expected resonances for the fundamental magnon mode at these harmonics. **b** Scheme of the experiment. **c** Calculated temporal evolution of the $\text{Fe}_{0.81}\text{Ga}_{0.19}$ lattice temperature induced by the 10-GHz optical excitation of the $\text{Fe}_{0.81}\text{Ga}_{0.19}/\text{GaAs}$ heterostructure at the pump excitation power $W=95$ mW (upper panel) and its Fourier spectrum (lower panel).

harmonics at the frequencies $f_n = nf_0$, where n is an integer. The harmonic amplitude decreases with the increase of n .

The idea of the experiments illustrated in Fig. 1a is to exploit the periodic thermal modulation for exciting coherent magnons and to monitor the magnetization precession by transient Kerr rotation (KR) measurements of the out-of-plane magnetization projection, δM_z , for various values of B . We expect a resonant increase of the precession amplitude at the resonances when $B=B_n$, which correspond to $f=f_n$. The expected values of B_n for the first three harmonics are shown in the right panel of Fig. 1a by the vertical arrows. The idea is analogous to the excitation of a harmonic oscillator with tunable eigenfrequency f by a periodic force, which acts on the oscillator with repetition rate f_0 . For magnetization precession, this force is generated by the modulated temperature $T(t)$, and the magnon eigenfrequency f is controlled by the external magnetic field.

Figure 2 shows the transient KR signals measured for $W=95$ mW and various values of B . The signals measured in the vicinity of the first resonance ($n=1$) have a harmonic shape. At these conditions, we fit the signals by a sine function $\delta M_z(t) = A_B \sin(\omega_1 t + \varphi_B)$ where $\omega_1=2\pi f_1$, and A_B and φ_B are the magnetic field-dependent amplitude and phase of the harmonic oscillations. Times $t=0$ and 100 ps correspond to excitation of the sample by the pump pulses. It is seen that the amplitude of the signal is maximal when $B=B_1=44$ mT, which corresponds to the first resonance $f=f_1$ (see Fig. 1a). In the vicinity of the resonance the phase changes from $\varphi_B = -\pi/2$ for $B < B_1$ to $\varphi_B = +\pi/2$ for $B > B_1$. At the resonance $\varphi_B \approx 0$. Similar results are observed for the signals measured in the vicinity of the second resonance ($n=2$). The amplitude of the oscillations at $B=B_2=250$ mT are 1.4 times smaller than for the first resonance and the same conclusions as for the first resonance can be made concerning the field dependences of the amplitude and phase of the signal around B_2 . Away from the resonances the signals are periodic but not harmonic. An example of a non-resonant signal measured at $B=190$ mT is presented in the right panel of Fig. 2. The amplitude of the signal is much smaller than in the case of resonance and the temporal shape is impossible to fit with a single sine function.

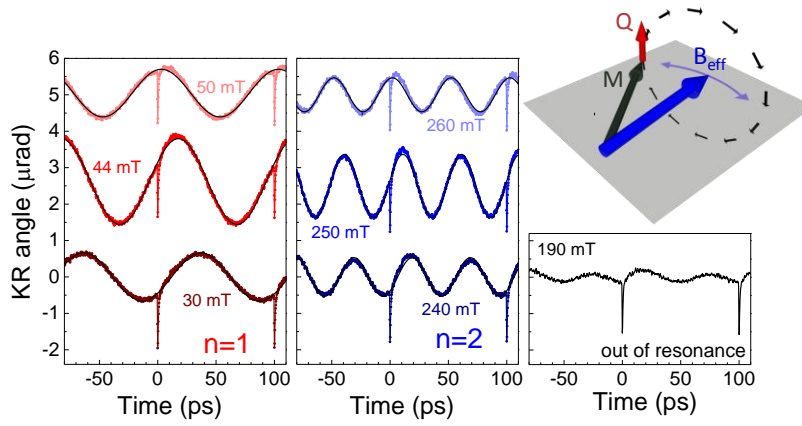


Figure 2. Transient Kerr rotation signals measured in the vicinity of the first (left panel) and second (central panel) resonances and at the intermediate magnetic field of 190 mT, corresponding to off-resonance (right panel). The amplification of the precession amplitude observed at $B=B_1=44$ mT and $B=B_2=250$ mT is due to thermally-induced resonant driving of the precession \mathbf{M} by the oscillating effective field B_{eff} . The torque \mathbf{Q} acting on the magnetization (see sketch at the top right) is maximal at the resonance conditions: $f=nf_0$.

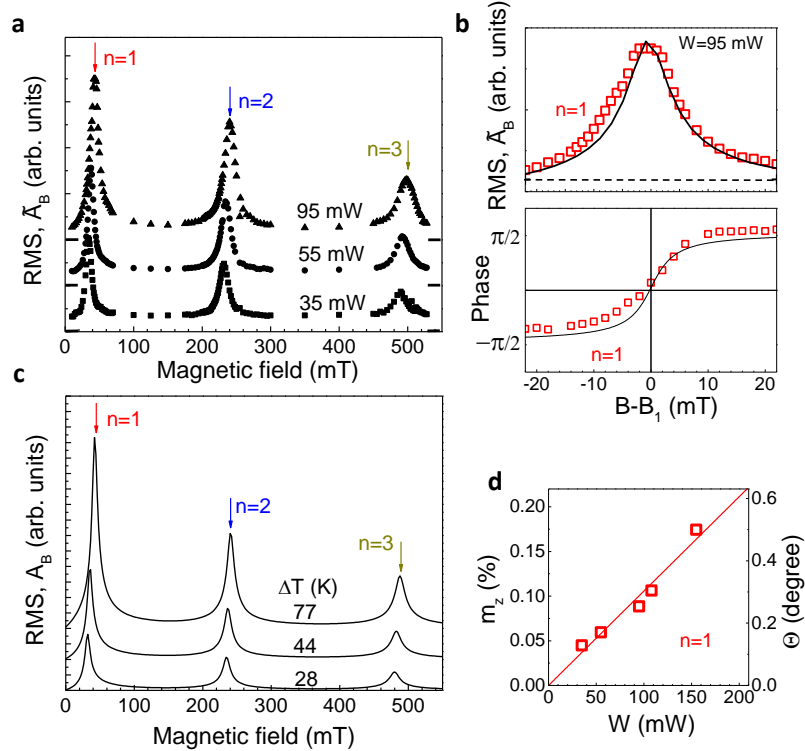


Figure 3. **a** Measured magnetic field dependences of the root mean square (RMS) amplitude of the Kerr rotation signal, \widetilde{A}_B , for three values of pump excitation power, W . The vertical arrows indicate the magnetic fields B_n at which the resonance condition $f=f_n$ is fulfilled; the horizontal bars indicate zero signal levels. **b** Measured (symbols) and calculated (solid lines) zoomed fragments of the field dependences of \widetilde{A}_B (upper panel) and the phase (lower panel) in the vicinity of the first resonance ($n=1$) for $W=95$ mW; the dashed horizontal line shows \widetilde{A}_B at the intermediate off-resonance field. **c** Calculated field dependences of the RMS precession amplitude for the background temperatures ΔT obtained from the experimental dependences in **a**. **d** Power dependence of the relative precession amplitude (left axis) and the corresponding precession angle (right axis) at the first resonance ($n=1$) when $f=f_0$.

To plot the dependence of the measured signal amplitude as a function of B we present the root-mean-square (RMS) amplitude \tilde{A}_B of the measured KR signal. The symbols in Fig. 3a show the field dependences $\tilde{A}_B(B)$ for three pump excitation powers W . It is clearly seen that the dependences have peaks at the resonant values of B_n corresponding to $n = 1, 2$ and 3 . Fig. 3b shows zoomed fragments of the field dependences of the amplitude and phase, respectively, obtained for the first resonance at $W=95$ mW. The 12-fold increase of \tilde{A}_B at the resonance condition is clearly seen by comparison with the out-of-resonance RMS amplitude shown by the horizontal dashed line in the upper panel of Fig. 3b. No peaks in the dependence of the precession amplitude on B are detected in the case of single pulse excitation, where \tilde{A}_B gradually decreases with the increase of B .

The values of the measured resonance fields B_n shift to slightly higher fields when W increases. We explain this shift by the heat-induced decrease of the magnon frequencies [13] and respective increase of the magnetic field value required for achieving the resonance conditions. We use the values of this shift to obtain the background temperature ΔT of the Galfenol film by comparison with the known dependence of $f(B)$ on temperature. Two dependences $f(B)$ calculated using the known dependence of the Galfenol magnetic parameters on temperature [13,14] are demonstrated in the right panel of Fig. 1a by the solid lines (for details see Supplementary Note 2). The corresponding values of the background temperature obtained from the experimentally measured shifts of the resonances are $\Delta T=28, 44$ and 77 K for $W=35, 55$ and 95 mW, respectively. They are 40% higher than the values calculated theoretically from the heat equations. We attribute this difference to the additional background heating by the probe beam that is not considered in the theoretical modeling.

Discussion

In the analysis, we consider thermal modulation of the magnetic anisotropy as the main mechanism for magnon excitation in our experiment and do not take into account other mechanisms (e.g. thermal strain). This approach is based on previous experiments and theoretical analysis where various mechanisms of laser-pulse induced excitation of magnons in Galfenol were considered [14]. We also exclude the effect of thermal gradients inside a ferromagnetic film (we estimate 4% temperature difference across the film). This gradient in special cases can induce ac-spin transfer [15,16] modulated at the laser repetition rate, f_0 . In our experiment, due to the uniform in-plane magnetization in a single thin ferromagnetic layer, this transfer does not produce a torque on the magnetization [17]. The dominating role of the thermal modulation of the magnetocrystalline anisotropy is also confirmed by the dependence of the precession amplitude excited by a single laser pulse on the direction of the external magnetic field. This dependence demonstrates a four-fold in-plane symmetry with a slight uniaxial distortion, which corresponds to the magnetocrystalline anisotropy of the studied layer [12].

We describe the effect of thermal modulation on the magnetization, \mathbf{M} , by considering the magnetization precession motion in a time-dependent effective field \mathbf{B}_{eff} as schematically shown in Fig. 2 [14]. The magnetization precession is described by the Landau-Lifshitz-Gilbert (LLG) equation [7]:

$$\frac{d\mathbf{m}}{dt} = -\gamma_0 \mathbf{m} \times \mathbf{B}_{\text{eff}}(t) + \alpha_0 \mathbf{m} \times \frac{d\mathbf{m}}{dt}, \quad (1)$$

where $\mathbf{m} = \mathbf{M}/M_0$ is the normalized magnetization and α_0 is the Gilbert damping parameter. The effective magnetic field is determined as $\mathbf{B}_{\text{eff}} = -\nabla_{\mathbf{m}} F_{\mathbf{M}}(\mathbf{m}, t)$, where $F_{\mathbf{M}}$ is the normalized free energy density [7]:

$$F_M(m) = -(\mathbf{m} \cdot \mathbf{B}) + B_d m_z^2 + K_1(m_x^2 m_y^2 + m_z^2 m_y^2 + m_x^2 m_z^2) - K_u(\mathbf{m} \cdot \mathbf{s})^2, \quad (2)$$

where the first term is the Zeeman energy, the second term is the demagnetization energy ($B_d = \frac{\mu_0 M_0}{2}$) and the following two terms describe the cubic and uniaxial magnetocrystalline anisotropy with respective coefficients K_1 and K_u , with the unit vector $\mathbf{s} \parallel [110]$ along the uniaxial anisotropy axis. In the chosen coordinate system, the x , y , and z axes correspond to the main crystallographic directions [100], [010] and [001] (normal to the layer plane), respectively. At equilibrium, i.e. without temperature modulation, the value of \mathbf{B}_{eff} determines the fundamental magnon frequency, while its direction sets the equilibrium orientation of the magnetization \mathbf{m} . The change of temperature alters \mathbf{B}_{eff} through the temperature dependent parameters M_0 , K_1 and K_u . Within the studied temperature range their dependence on T is linear [13]: $X = X^{RT} + \beta_X(T - T_0)$, where $X = M_0, K_1$ or K_u , the index RT indicates the room-temperature values and β_X is the corresponding thermal coefficient. The room temperature values $M_0^{RT} = 1.96$ T, $K_1^{RT} = 20$ mT and $K_u^{RT} = 9$ mT for our sample are found from fitting the experimental dependence $f(B)$ (shown in the right panel of Fig 1a) [12,14]. The thermal coefficients, $\beta_{M_0} = -0.97$ mT/K, $\beta_{K_1} = -0.046$ mT/K and $\beta_{K_u} = -0.025$ mT/K for Galfenol are taken from previous studies [13,14]. The Gilbert damping coefficient $\alpha_0 = 0.006$ is obtained from the precession kinetics excited by a single laser pulse.

The modulation amplitude $\delta T \ll \Delta T$ and for solving Eq. (1) we assume that the magnitude of \mathbf{B}_{eff} is constant and the temperature modulation affects only its direction. We also consider only the ground magnon mode with zero wave vector, i.e. we assume a uniform precession, due to the large diameter (17 μm) of the excitation spot, which limits the in-plane wave vector of magnons to $q_{\parallel} \leq 4700 \text{ cm}^{-1}$. In the 5-nm thick Galfenol layer the frequency range for such q_{\parallel} does not exceed 270 MHz [18, 19], which is clearly below the 500-MHz spectral width of the fundamental magnon mode. For details of the magnon dispersion and contribution of magnons with finite wave vectors in a 100-nm thick layer, see Supplementary Note 4.

With these assumptions, the LLG equation can be reduced to a system of equations (see the Methods section for details) for the magnetization components, where the thermal modulation of the anisotropy coefficients alters the direction of \mathbf{B}_{eff} and generates a tangential driving torque, \mathbf{Q} , acting on the magnetization [14] as schematically shown in the inset of Fig. 2. The vector \mathbf{B}_{eff} follows the temporal temperature evolution $T(t)$ shown in Fig. 1c, which can be written as sum of background heating and a Fourier series expansion for the small periodic temperature modulation:

$$T(t) = T_0 + \Delta T + \delta T \sum_{n=1}^{\infty} u_n \sin(\omega_n t + \psi_n). \quad (3)$$

Here the amplitude and phase of the n^{th} harmonic are $u_n = \frac{2}{\pi} \frac{\omega_1 \tau_0}{\sqrt{1 + \omega_n^2 \tau_0^2}}$ and

$\psi_n = \arctan\left(\frac{1}{\omega_n \tau_0}\right)$, respectively, $\omega_n = 2\pi f_n$, τ_0 is the characteristic cooling time of the Galfenol layer, which is determined by the thermal boundary resistance, R , at the interface with GaAs [17]. The solution of the linearized Eq. (1) for the δm_z - component expanded as a Fourier series has the form:

$$\delta m_z(t) = \sum_{n=1}^{\infty} A_n(B) \sin(\omega_n t + \varphi_n(B)), \quad (4)$$

where $A_n(B)$ and $\varphi_n(B)$ are the time-independent amplitude and phase for the n^{th} harmonic. Like in the case of a simple harmonic oscillator, at the resonant conditions $f(B) = f_n$ the precession amplitude reaches maximum with zero phase-shift relative to the driving force $\varphi_n(B) \approx 0$. The analytical expressions for $A_n(B)$ and $\varphi_n(B)$ are presented in the Methods section.

Figure 3c shows the field dependences of the RMS amplitude of the calculated $\delta m_z(t)$ for three values of the background temperature ΔT which correspond to the W indicated near the experimentally measured data in Fig. 3a. The agreement of the measured and calculated spectral shapes is explicitly demonstrated in the zoomed dependences of the RMS amplitude and phase in Fig. 3b, where the calculated dependences (solid lines) for $n=1$ are presented together with the experimental values. Good agreement is observed also for higher n and W .

The measured power dependence of the resonant magnon amplitude for $n=1$ in the studied sample is shown in Fig. 3d. The precession amplitudes are obtained from the absolute values of the Kerr rotation angle in the transient Kerr signals [12]. The field independent small amplitude background, which is due to the response of the electron system and not related to the magnetization [21], has been subtracted from the experimental values. At $W=100$ mW the precession amplitude reaches 0.1% of the saturation magnetization M_0 . To get this value, the parameters of the magnetic anisotropy have to be modulated by the oscillating temperature with the amplitude $\delta T=0.54$ K. This is in perfect agreement with the values obtained by solving the thermal equations which for the same power give $\delta T=0.49$ K. The achieved precession amplitude, which corresponds to the precession angle $\Theta \approx 0.25^\circ$ (with the ellipticity of 0.2) and the generated ac- induction $\Delta M_z \sim 1$ mT, is large enough for prospective spintronics applications: detection of spin currents by spin pumping [22,23]; manipulating single spin states of NV-centers in nanodiamonds by microwave magnetic fields [24]; excitation of propagating spin waves in magnonic devices [25].

For the practical use of resonant energy harvesting in a device excited optically or electrically, it is important to achieve high efficiency of the transformation of the modulated part of the thermal energy into the oscillations of magnetization. This efficiency is defined by the ratio of the magnetization angle Θ of precession and the power W injected into a device. In our experiment, we demonstrate $\Theta/W = 2.5^\circ/\text{W}$ which is only one order of magnitude less than the efficiency of conventional mesoscopic microwave devices [26] and of the same order as devices utilizing surface acoustic waves for spin pumping [27]. At resonance, the magnetization precession remains harmonic up to the maximum used power, and, thus, non-linear (anharmonic) effects do not affect the transformation efficiency. However, the shift of the resonance frequency with the increasing ΔT at higher W affects the linear power dependence of the precession amplitude at fixed magnetic field. This temperature-induced “nonlinearity” is known from the conventional microwave experiments on ferromagnetic resonance [28]. The effect of this nonlinearity is very weak in the studied structure. For instance, for the second resonance ($n=2$) the 20%-change of the background temperature without changing thermal modulation amplitude results in a $\sim 3\%$ decrease of the precession amplitude. Thus, stability of the background temperature is not critical for the suggested concept.

The dependences of δT on the parameters of the used structure and materials define the efficiency of the heat transfer to the magnons. For optical excitation, shorter penetration depths and smaller heat capacities of the ferromagnetic layer increase δT and correspondingly Θ/W . It is convenient to define the dimensionless resonant harvesting efficiency, $\zeta = \delta T/\Delta T$, which governs the ratio of the useful temperature modulation δT relative to the parasitic heating, ΔT . Obviously, it is favorable to have ζ as large as possible. For instance, faster cooling to the bulk of the substrate leads to an increase of δT with a simultaneous decrease of ΔT and correspondingly to an increase of ζ . In our particular experiment, where both the $\text{Fe}_{0.81}\text{Ga}_{0.19}$ nanolayer and the GaAs substrate are excited optically we get $\zeta \sim 10^{-2}$. The value of ζ increases with the decrease of the thickness of ferromagnetic layer and the increase of substrate

thermoconductivity (see Supplementary Note 3). For instance, for the same ferromagnetic layer on a silicon substrate ζ increases by a factor of 1.5. An efficient way to increase ζ and the efficiency of the heat-magnon transfer would be to use a multilayer structure where ΔT is governed by the rapid escape of heat to the substrate while the high frequency thermal waves which define δT are localized inside or in the vicinity of the harvester layer. To demonstrate that the concept is applicable for electrical nanodevices we have considered the case of a thin conducting layer (e.g. graphene) where Joule heat can be generated as a result of passing GHz current pulses and transferred to the ferromagnetic harvester through a thin spacer layer. For high efficiency the spacer layer should have high thermal conductivity while the ferromagnetic layer should have low specific heat capacity. In the example presented in the Supplementary Note 3 we get $\zeta=4\times 10^{-3}$.

In our experiments, we excite resonances up to 30 GHz. To reach higher, sub-THz frequencies, the corresponding bandwidth should be available for both temperature and magnon modulation. For temperature modulation, we refer to the picosecond acoustic experiment [4] where the temperature in a 12-nm Al film was modulated at a frequency up to 400 GHz. The thermal properties of ferromagnetic metals do not differ much from normal metals and thus similar modulation in thin films is achievable. For optical excitation of metals, it is essential that optically excited hot electrons pass their energy to the lattice in a time less than 1 ps. Theoretically, for the parameters fixed as above the amplitude of the temperature oscillations is proportional to the laser power and inversely proportional to the frequency up to sub-THz frequencies. For the magnons in thin (Fe,Ga) films, narrow-band precession with frequencies up to 100 GHz was demonstrated at strong magnetic fields [12]. Moreover, novel metallic ferrimagnetic materials (e.g. Mn-Te compounds) possess narrow magnon resonances at frequencies up to hundreds of GHz at low magnetic fields [27]. At the lower frequency end, there is no limit for temperature modulation while for magnons the lower frequency varies from hundreds of MHz (e.g. for garnets) up to several GHz in metallic ferromagnets. The available choice of a proper magnetic material is not limited to the Galfenol used in our study. This novel ferromagnet is actively studied nowadays [30] and presents a good example for realization of the demonstrated concept due to its pronounced magnetocrystalline anisotropy and narrow magnon resonances (long lifetime of precession). However, other ferro- and ferrimagnetic materials possessing similar properties will also work as resonant harvesters for transferring parasitic heat modulated at high frequencies to magnons.

To conclude, we have demonstrated how the heat generated during 10 GHz pulsed optical excitation is used for the excitation of resonant magnons. The amplitude of the magnetization precession at the fundamental magnon frequency increases enormously when the repetition rate of the optical pulses is equal to the magnon frequency. The resonances also occur at the higher harmonic frequencies, i.e. 20 and 30 GHz. An amplitude of the temperature modulation of order ~ 0.1 K is sufficient to generate AC magnetization with an amplitude of 1 mT [31] which is sufficient to be exploited in various applications including information and quantum technologies. The concept of resonant heat transfer can be considered as a prospective method to generate magnons in ferromagnetic layers deposited on processors and other microchips operating at GHz and sub-THz clock frequencies.

Methods

Pump-probe measurements with 10-GHz repetition rate: We used two synchronized Titanium sapphire lasers (Taccor x10 and Gigajet 20c from Laser Quantum) generating 50 fs pulses with repetition rates of 10 GHz (pump) and 1 GHz (probe) at center wavelengths of 810 and 780 nm, respectively. The beams were focused onto the sample using a reflective microscope objective with

a magnification factor of 15 comprising 4 sectors through which light could enter and exit the objective [32]. The incidence angles of the laser beams are 17 °. The spot diameters for the pump and probe beams were set to 17 μm and 14 μm , respectively. The diameters are defined at the $1/e^2$ -level of the Gaussian spatial energy distributions. The coherent response of the magnetization was measured by monitoring the polar Kerr rotation of the reflected probe pulses using a differential scheme based on a Wollaston prism and a balanced optical receiver with 10-MHz bandwidth. Temporal resolution was achieved by means of an asynchronous optical sampling (ASOPS) technique [33], where we used an offset frequency of 20 kHz between the 10 GHz laser and the 10th harmonics of the 1-GHz laser in order to resolve the transient signals in 100 ps time window between pump pulses with the time resolution of 50 fs. The sample was mounted between the poles of a dipole electromagnet.

Measurements of the magnon spectrum with single pulse excitation. The magnon spectrum of the studied sample was obtained by a conventional magneto-optical pump-probe scheme based on two mode-locked Erbium-doped ring fiber lasers (FemtoFiber Ultra 780 and FemtoFiber Ultra 1050 from Toptica). The lasers generate pulses of 150-fs duration with a repetition rate of 80 MHz at wavelengths of 1046 nm (pump pulses) and 780 nm (probe pulses). The magnetization precession was excited by the pump pulses with energy of 3 nJ per pulse focused on the Galfenol film surface to a spot of 17 μm diameter. The linearly polarized probe pulses with energy of 30 pJ per pulse hitting at normal incidence to the sample surface were focused to a spot of 1 μm diameter in the center of the pump spot. The coherent response was measured by transient polar Kerr rotation in the same way as for the 10-GHz measurements. Temporal resolution was achieved also by the ASOPS technique with a frequency offset of 800 Hz, which in combination with the 80-MHz repetition rate allowed measurement of the time-resolved signals in the time window of 12.5 ns with 150-fs time resolution. The magnon spectra and the magnetic field dependence of the central frequency were obtained by fast Fourier transforming the corresponding transient Kerr rotation signals.

Modeling of temperature evolution. In the case of periodic laser pulse excitation, the temperature oscillates around the background temperature $T_0 + \Delta T$ with amplitude δT . The amplitude δT is estimated by solving the standard heat equations for the lattice temperatures of $\text{Fe}_{0.81}\text{Ga}_{0.19}$ and GaAs for periodic excitation by laser pulses using Comsol Multiphysics® [34] (see Supplementary Note 1). We estimate the background heating ΔT from the solution of the 3D stationary heat equation for cw-laser excitation (see Supplementary Note 2). We use the following parameters for GaAs [35]: refractive index $3.7+i0.09$ which results in an absorption length of 740 nm; heat capacity $1.76 \times 10^6 \text{ Jm}^{-3}\text{K}^{-1}$ and thermal conductivity $55 \text{ Wm}^{-1}\text{K}^{-1}$ [36,37]. We assume that the optical and thermal parameters of $\text{Fe}_{0.81}\text{Ga}_{0.19}$ are close to the parameters of Fe: refractive index $2.9+i3.4$ [38]; heat capacity $3.8 \times 10^6 \text{ Jm}^{-3}\text{K}^{-1}$ and thermal conductivity $80 \text{ Wm}^{-1}\text{K}^{-1}$ [39]. As a result the reflection coefficient of the (Fe,Ga)/GaAs heterostructure is 0.4 and the absorption coefficients for the $\text{Fe}_{0.81}\text{Ga}_{0.19}$ layer and GaAs substrate are 0.1 and 0.49, respectively. The calculated values of ΔT and δT at the excitation power $W=95 \text{ mW}$ are 48 K and 0.47 K, respectively.

In our calculations, we consider the thermal boundary resistance, R , which determines the flux through the $\text{Fe}_{0.81}\text{Ga}_{0.19}$ /GaAs interface [17]. In order to estimate R , we measured the reflectivity signal from the studied structure in the case of low-frequency (80-MHz) laser excitation. Using the experimentally observed decay time of the transient reflectivity $\tau_0 = 200 \text{ ps}$ we found the thermal boundary resistance $R=10^{-8} \text{ m}^2\text{KW}^{-1}$. HIM

Modelling the periodic laser pulse-induced magnetization precession. To calculate the magnetization precession amplitudes $A_n(B)$ and phases $\varphi_n(B)$, we apply the approach developed in Ref. [14] where the detailed theory of magnetization precession due to ultrafast heating of a Galfenol film was considered. We analyze the precession by rewriting the LLG equation in a spherical coordinate system with in-plane azimuthal angle, ϕ , and polar angle, θ , ($\theta = 0$ corresponds to the layer normal, z), which describes the direction of the normalized magnetization, \mathbf{m} . Assuming that the changes of $\delta\phi$ and $\delta\theta$ from the equilibrium angles ϕ_0 and θ_0 are small and induced by the

modulation of the cubic and uniaxial anisotropy constants, the LLG equation in linear approximation has the form:

$$\frac{\partial \delta \phi}{\partial t} = \gamma_0 F_{\theta \theta} \delta \theta + \alpha_0 \frac{\partial \delta \theta}{\partial t}, \quad (5)$$

$$\frac{\partial \delta \theta}{\partial t} = \gamma_0 F_{\phi \phi} \delta \phi - \gamma_0 F_{\phi K_1} \delta K_1 - \gamma_0 F_{\phi K_u} \delta K_u(t) - \alpha_0 \frac{\partial \delta \phi}{\partial t},$$

Where the $F_{i,j} = \frac{\partial^2}{\partial i \partial j} F_M$ ($i, j = \theta, \phi, K_1, K_u$) are calculated for the equilibrium (in-plane) orientation of \mathbf{m} , $\phi_0(\mathbf{B}, T)$, $\theta_0 = \pi/2$ and α_0 is the Gilbert damping parameter. At the in-plane equilibrium orientation of \mathbf{m} , $F_{\theta \phi} = F_{\theta K_1} = F_{\theta K_u} = 0$ and there is no torque due to the thermal change of M_0 .

In Eq. (4) the precession amplitude and phase are determined as $A_n(B) = \sqrt{a_n^2(B) + b_n^2(B)}$ and $\varphi_n(B) = \arctan(a_n(B)/b_n(B))$, where $a_n(B) = (-\omega_n \xi Q_n^b + 2\tau_M^{-1} \omega_n^2 Q_n^a)/G$ and $b_n(B) = (\omega_n \xi Q_n^a + 2\tau_M^{-1} \omega_n^2 Q_n^b)/G$, with $G = \xi^2 + 4\omega_n^2 \tau_M^{-2}$, and $\xi = \omega_n^2 - \omega^2$. Here $\omega = 2\pi f(B)$ and $\tau_M^{-1} = \alpha_0 \gamma_0 (F_{\theta \theta} + F_{\phi \phi})/2$ are the field-dependent frequency and decay time of the fundamental magnon mode [12]. The Fourier series expansion coefficients of the effective driving force Q_n^a and Q_n^b are determined by the temporal modulation of the temperature given by Eq. (2) and are equal to $Q_n^a = \frac{2}{\pi} \cdot \frac{\omega_1 \tau_0}{1 + \omega_n^2 \tau_0^2} Q$ and $Q_n^b = \frac{2}{\pi} \cdot \frac{\omega_1 \omega_n \tau_0^2}{1 + \omega_n^2 \tau_0^2} Q$, where $Q = \gamma_0 (\sin(4\phi_0) \beta_{K_1}/2 - \cos(2\phi_0) \beta_{K_u}) \delta T$.

References

- [1] Benenti, G., Casati, G., Saito, K. & Whitney, R. S., Fundamental aspects of steady-state conversion of heat to work at the nanoscale. *Phys. Rep.* **694**, 1–124 (2017).
- [2] Bell, A. G., Upon the production of sound by radiant energy. *Philos. Mag. J. Sci.* **11**, 510–528 (1881).
- [3] Manomar, S. & Razansky, D., Photoacoustics: a historical review. *Adv. Opt. Photonics* **8**, 586–617 (2016).
- [4] Klieber, C., Peronne, E., Katayama, K., Choi, J., Yamaguchi, M., Pezeril, T. & Nelson, K. A., Narrow-band acoustic attenuation measurements in vitreous silica at frequencies between 20 and 400 GHz. *Appl. Phys. Lett.* **98**, 211908 (2011).
- [5] Chumak, A. V., Vasyuchka, V. I., Serga A. A., & Hillebrands B., Magnon spintronics. *Nature Phys.*, **11**, 453 – 461 (2015).
- [6] Yi Li et al., Strong Coupling between magnons and microwave photons in on-chip ferromagnet-superconductor thin-film devices. *Phys. Rev. Lett.* **123**, 107701 (2019).
- [7] Gurevich, A.G. & Melkov, G.A., Magnetization oscillations and waves (CRC-Press, Boca Raton, 1996).
- [8] van Kampen, M., et al. All-optical probe of coherent spin waves, *Phys. Rev. Lett.* **88**, 227201 (2002).
- [9] Vomir, M., Andrade, L. H. F., Guidoni, L., Beaupaire, E., & Bigot, J.-Y., Real space trajectory of the ultrafast magnetization dynamics in ferromagnetic metals. *Phys. Rev. Lett.* **94**, 237601 (2005).
- [10] Frait. Z. & MacFaden, H., Ferromagnetic resonance in metals. Frequency dependence. *Phys. Rev.* **139**, A1173 – A1181 (1965).
- [11] Restorff, J.B. et al., Tetragonal magnetostriction and magnetoelastic coupling in Fe-Al, Fe-Ga, Fe-Ge, Fe-Si, Fe-Ga-Al, and Fe-Ga-Ge alloys. *J. Appl. Phys.* **111**, 023905 (2012).
- [12] Scherbakov, A.V. et al., Optical excitation of single- and multimode magnetization precession in Fe-Ga nanolayers. *Phys. Rev. Appl.* **11**, 031003 (2019).
- [13] Clark, A. E. et al., Temperature dependence of the magnetic anisotropy and magnetostriction of Fe_{100-x}Ga_x (x=8.6, 16.6, 28.5). *J. of Appl. Phys.* **97**, 10M316 (2005).
- [14] Kats, V. N. et al., Ultrafast changes of magnetic anisotropy driven by laser-generated coherent and noncoherent phonons in metallic films, *Phys. Rev. B* **93**, 214422 (2016).

- [15] Melnikov, A. et al., Ultrafast Transport of Laser-Excited Spin-Polarized Carriers in Au/Fe/MgO(001). *Phys. Rev. Lett.* **107**, 076601 (2011).
- [16] Kimling, J. et al., Picosecond spin Seebeck effect, *Phys. Rev. Lett.* **118**, 057207 (2017).
- [17] Razdolskii, I., et al. Nanoscale interface confinement of ultrafast spin transfer torque driving non-uniform spin dynamics, *Nature Commun.* **8**, 15007 (2017).
- [18] Kamimaki, A., Iihama, S., Sasaki, Y., Ando, Y., & Mizukami, S. Reciprocal excitation of propagating spin waves by a laser pulse and their reciprocal mapping in magnetic metal films. *Phys. Rev. B* **96**, 014438 (2017).
- [19] Khokhlov, N. E. et al., Optical excitation of propagating magnetostatic waves in an epitaxial gallium film by ultrafast magnetic anisotropy change. *Phys. Rev. Appl.* **12**, 044044 (2019).
- [20] Krenzer, B., Hanisch, A., Duvenbeck, A., Rethfeld, B., and Horn-von Hoegen, M. Heat transport in nanoscale heterosystems: A Numerical and Analytical Study. *J. Nanomat.* **2008**, 590609 (2008).
- [21] Razdolski, I. et al., Analysis of the time-resolved magneto-optical Kerr effect for ultrafast magnetization dynamics in ferromagnetic thin films. *J. Phys. C* **29**, 174002 (2017).
- [22] Ando, K. et al., Inverse spin-Hall effect induced by spin pumping in metallic system. *J. Appl. Phys.* **109**, 103913 (2011).
- [23] Weiler M. et al., Spin pumping with coherent elastic waves. *Phys. Rev. Lett.* **108**, 176601 (2012).
- [24] Fuchs, G. D. et al., Excited-state spectroscopy using single spin manipulation in diamond. *Phys. Rev. Lett.* **101**, 117601 (2008).
- [25] Demidov, V.E. et al., Excitation of coherent propagating spin waves by pure spin currents. *Nature Commun.* **7**, 10446 (2016).
- [26] Gupta, S. et al., Important role of magnetization precession angle measurement in inverse spin Hall effect induced by spin pumping. *Appl. Phys. Lett.* **110**, 022404 (2017).
- [27] Weiler, M. Spin Pumping with Coherent Elastic Waves. *Phys. Rev. Lett.* **108**, 176601 (2012).
- [28] Damon, R. W., Thermally-induced nonlinear effects in the ferromagnetic resonance. *Phys. Stat. Sol.* **8**, K89-K93 (1965).
- [29] Mizukami, S. Long-lived ultrafast spin precession in manganese alloys films with a large perpendicular magnetic anisotropy. *Phys. Rev. Lett.* **106**, 117201 (2011).
- [30] Parkes, D. E. et al., Magnetostrictive thin films for microwave spintronics. *Sci. Reports.* **3**, 2220 (2013).
- [31] Salasyuk, A.S. et al., Generation of a localized microwave magnetic field by coherent phonons in a ferromagnetic nanograting. *Phys. Rev. B* **97**, 060404(R) (2018).
- [32] Kreilkamp, L. E. et al., Terahertz dynamics of lattice vibrations in Au/CdTe plasmonic crystals: photoinduced segregation of Te and enhancement of optical response. *Phys. Rev. B* **93**, 125404 (2016).
- [33] Bartels, A., Hudert, F., Janke, C., Dekorsy, T. & Köhler, K., Femtosecond time-resolved optical pump-probe spectroscopy at kilohertz-scan-rates over nanosecond-time-delays without mechanical delay line. *Appl. Phys. Lett.* **88**, 041117 (2006).
- [34] COMSOL Multiphysics® v. 5.4. <http://www.comsol.com>. COMSOL AB, Stockholm, Sweden.
- [35] Aspnes, D. E., Kelso, S. M., Logan, R. A., and Bhat, R., Optical properties of Al_xGa_{1-x}As. *J. App. Phys.* **60**, 754- 767(1986).
- [36] Chen, B., Fu, X. Tang, J., Lysevych, M., Tan, H. H., Jagadish, C., Zewail, A. H., Dynamics and control of gold-encapped gallium arsenide nanowires imaged by 4D electron microscopy. *Proc. Nat. Acad. Sci.* **114**, 12876 - 12881, (2017).
- [37] Carlson, R. O., Slack, G. A., Silverman, S. J., Thermal conductivity of GaAs and GaAs_{1-x}P_x laser semiconductors. *J. App. Phys.* **36**, 505 – 507 (1965).
- [38] Johnson, P. B. and Christy, R. W., Optical constants of transition metals: Ti, V, Cr, Mn, Fe, Co, Ni, and Pd. *Phys. Rev. B* **9**, 5056 - 5070 (1974).
- [39] Lide, D.R., CRC Handbook of Chemistry and Physics (CRC Press, Boca Raton, FL, 2003).

Acknowledgements

We are grateful to Ilya Razdolski for fruitful discussions. The work was supported by the Bundesministerium für Bildung und Forschung through the project VIP+ "Nanomagnetron" and by the Deutsche Forschungsgemeinschaft and the Russian Foundation for Basic Research (Grants No. 19-52-12065) in the frame of the International Collaborative Research Center TRR 160. The cooperation between TU Dortmund, the Lashkaryov Institute and the Ioffe Institute was supported by the Volkswagen Foundation (grant no. 97758).

Author contributions

M.K. constructed the experimental setup, carried out the experiment and performed the data analysis. A.V.S., I.A.A, and A.V.A. designed the experiment and supervised the experiment and theoretical modeling, T.L.L., S.M.K and V.E.G. performed theoretical analysis and numerical modeling, A.W.R. and D.P.P. designed and deposited the Galfenol samples, D.P.P. characterized the Galfenol samples, M.K., A.V.S., T.L.L, S.M.K, V.E.G., I.A.A, A.W.R., A.V.A and M.B. discussed the results and wrote the manuscript.

Competing interests

The authors declare no competing interests.

Data availability

The data that supports the plots within this paper and other findings of this study are available from the corresponding authors upon reasonable request.

Supplementary Information

Note 1. Modeling of heat transport for periodically pulsed optical excitation

In order to describe the heat transport in the system of a plane metallic film on a substrate we used the one-dimensional two-temperature model for the lattice heating temperatures of the film, T_f , and the substrate, T_s :

$$c_f \frac{\partial T_f}{\partial t} - \kappa_f \frac{\partial^2 T_f}{\partial z^2} = F_p A_f g(t) \frac{dS}{dz}, \quad (S1)$$

$$c_s \frac{\partial T_s}{\partial t} - \kappa_s \frac{\partial^2 T_s}{\partial z^2} = F_p A_s g(t) \frac{dS}{dz}, \quad (S2)$$

where c_j , κ_j , and A_j are the heat capacity, thermal conductivity, and fraction of absorbed optical energy relative to the incident excitation energy (further referred to as absorption coefficients), respectively ($j = f, s$). The pump laser pulse fluence $F_p = 2W/(f_0\pi r^2)$, where W is the average laser power, $f_0 = 10$ GHz is the laser repetition rate, and r is the radius of the pump spot defined by $1/e^2$ of the intensity. The function, $g(t) = \frac{2}{\tau_p} \sqrt{\frac{2}{\pi}} \sum_{n=1}^{\infty} \exp\left(-2 \frac{(t - \frac{n-1}{f_0})^2}{\tau_p^2}\right)$, describes the temporal evolution of the laser pulses with duration, τ_p , and repetition rate, f_0 . Everywhere throughout the Supplementary Information, we chose the coordinate system with the direction of the z-axis pointing from the substrate to the film.

We found the absorption coefficients from the solution of Maxwell equations for the three-layer (air/metal/substrate) system:

$$A_f = 1 - \left| \frac{(k_a k_f - k_f k_s) \cos(k_f h) - i(k_a k_s - k_f^2) \sin(k_f h)}{(k_a k_f + k_f k_s) \cos(k_f h) - i(k_a k_s + k_f^2) \sin(k_f h)} \right|^2 - A_s, \quad (S3)$$

$$A_s = \text{Re}(n_s) \left| \frac{2k_a k_f}{(k_a k_f + k_f k_s) \cos(k_f h) - i(k_a k_s + k_f^2) \sin(k_f h)} \right|^2, \quad (S4)$$

where $k_j = k_a n_j$ is the complex wave vector of light in the air ($j=a$), film ($j=f$), and substrate ($j=s$), n_j is the complex refractive index, h is the thickness of the film.

The function $dS(z)/dz$ describes the spatial distribution of the energy density deposition by the pump light, which penetrates into the medium. More specifically, $S(z)$ is normalized to the value of the flux of electromagnetic energy at the metal surface. We used COMSOL Multiphysics® [S1] to calculate $S(z)$.

The equations (S1)-(S4) must be complemented by the boundary conditions. At the interface between the film and substrate (i.e. at $z = 0$), the boundary conditions read:

$$\kappa_f \frac{\partial T_f}{\partial z} \Big|_{z=0} = \kappa_s \frac{\partial T_s}{\partial z} \Big|_{z=0} = (T_f - T_s)/R, \quad (S5)$$

where R is the thermal boundary resistance. At the interface of air and film, we assumed a zero heat flux boundary condition, i.e. $\kappa_f \frac{\partial T_f}{\partial z} \Big|_{z=h} = 0$. We take the thickness of the substrate large enough to minimize the impact of any boundary condition at the back side of the substrate.

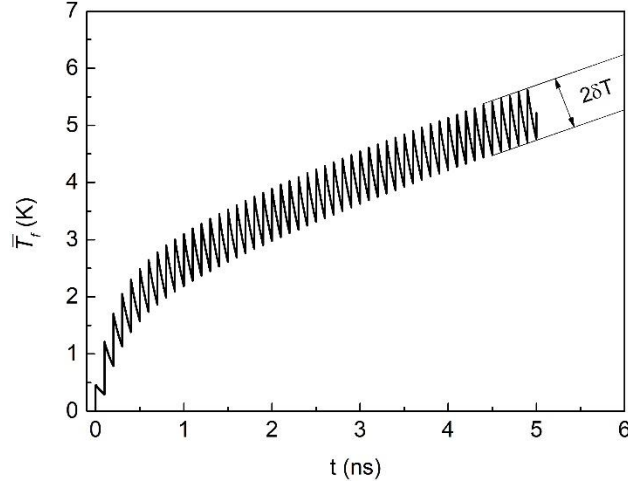


Fig. S1. The temporal evolution of the average temperature $\bar{T}_f(t)$ for periodic laser pulse excitation with average power $W=95$ mW incident on the FeGa film with a thickness $h=5$ nm deposited on the GaAs substrate.

The described approach was implemented in COMSOL Multiphysics®. The example of the average lattice heating temperature of the film $\bar{T}_f = \int_0^h \frac{T_f dz}{h}$ for $W = 95$ mW, $r = 8.5$ μ m is shown in Fig. S1. One can see that the temperature oscillates with the excitation frequency $f_0=10$ GHz around a slowly increasing background. Here we want to mention that our calculations show that in the discussed one-dimensional (1D) heat transport problem the background temperature does not reach a stationary value but, diverges with time. However, as one can clearly see from Fig. S1, the amplitude of thermal oscillations, δT , converges very quickly. In order to estimate the stationary background temperature ΔT we solved analytically the stationary 3D problem, see the next Supplementary Note.

Note 2. Estimation of background temperature ΔT

Theory

In order to calculate the background temperature rise ΔT , we solved analytically the stationary 3D heat equation for T_s . Taking into account that the optical excitation energy is absorbed in a layer with a thickness much less than the radius of excitation at the surface, we may assume that the thermal source is located at the interface ($z=0$). Then the equation and boundary condition may be written as:

$$\left(\frac{\partial^2}{\partial x^2} + \frac{\partial^2}{\partial y^2} + \frac{\partial^2}{\partial z^2} \right) T_s = 0, \quad (\text{S6})$$

and

$$\kappa_s \frac{\partial T_s}{\partial z} \Big|_{z=0} = (A_f + A_s) I \exp\left(-2 \frac{x^2 + y^2}{r^2}\right), \quad (\text{S7})$$

where I is the laser intensity which is related to the laser power by

$$W = I \iint_{-\infty}^{\infty} \exp\left(-2 \frac{x^2 + y^2}{r^2}\right) dx dy = I \frac{\pi r^2}{2}. \quad (\text{S8})$$

The analytical solution of these equations at $z=0$ and at the center of the laser beam ($x=y=0$) reads

$$\Delta T = \frac{(A_f + A_s)W}{\sqrt{2\pi\kappa_s r}}. \quad (\text{S9})$$

It is obvious that for optical excitation from the side of the film (absorption length smaller in the metal than in the substrate) we have $T_f > T_s$ because of the boundary resistance. We estimate the jump of the temperature at the interface, using the boundary condition (S5). In this case, the temperature jump at the interface of the film and substrate is given by

$$(T_f - T_s)|_{z=0} = (A_f + A_s)IR = (A_f + A_s)W \frac{2R}{\pi r^2}. \quad (\text{S10})$$

For the parameters of our experiment, the temperature (S9) is 10 times larger than the temperature jump (S10). Thus, the effect of the temperature jump can be neglected.

Experiment

We also derive the background temperature ΔT from the measured dependences of the resonance fields B_1 , B_2 , and B_3 on W . For this we take the derivatives dB/dW from the experimental data in Fig. 3a and compare them with the calculated derivatives dB/dT [see theoretical curves $f(B)$ in Fig. 1(a) of the main text]. As a result, we get the values for $dT/dW=(dB/dW)/(dB/dT)$ for the three resonant frequencies 10, 20 and 30 GHz. The results are presented in the Table S1.

Table S1. The measured values of the resonant magnetic fields B_1 , B_2 , and B_3

Excitation Power (mW)	Resonant Fields (mT)		
	10 GHz	20 GHz	30 GHz
35	34	232	490
55	38	234	492
95	42	240	498

Table S2. Power and temperature derivatives for the three resonant frequencies

	10 GHz	20 GHz	30 GHz
dB/dW (mT/mW)	0.13	0.13	0.13
dB/dT (mT/K)	0.19	0.13	0.16
dT/dW (K/mW)	0.7	0.9	0.7

Table S3. Values of the background temperature rise.

Power (mW)	ΔT (K)	
	Calculated	Extracted from experiment
35	18	28±2
55	28	44±3
95	48	77±5

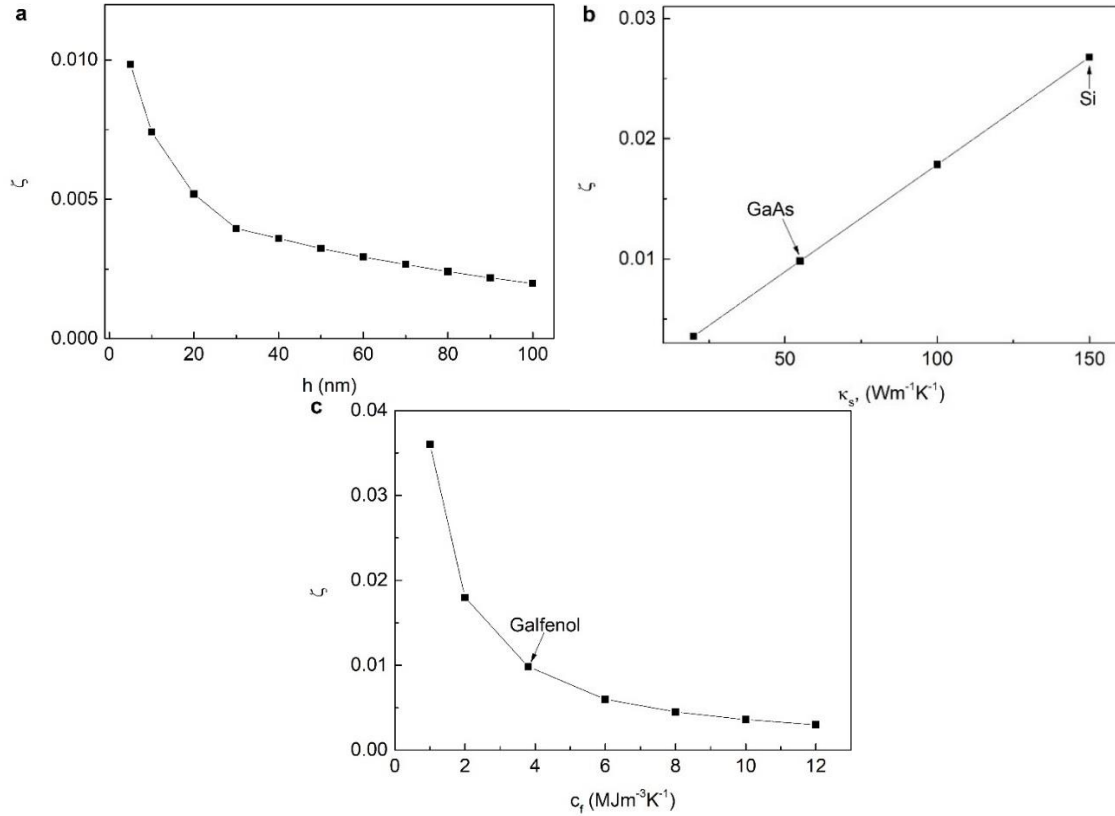


Fig. S2. Dependencies of the efficiency parameter, ζ on h (a), κ_s (b), and c_f (c).

The average value for $dT/dW = 810 \pm 50$ K/W. The estimated temperature rise $\Delta T = (dT/dW)W$ for the three values of W are presented in Table S3 and compared with the theoretical values. The difference between the values calculated and extracted from the experiments is less than 40%. This difference may be due to additional heating by the probe which is not included into the theoretical calculations.

Note 3. Dependence of $\zeta = \delta T / \Delta T$ on parameters and design of the device

Figure S2 shows the dependencies of the dynamical harvesting efficiency $\zeta = \delta T / \Delta T$ on the film thickness and thermal conductivity of the substrate. The value of ζ does not depend on power, because both δT and ΔT depend linearly on W . As one can see from Fig. S2a, ζ decreases with increasing film thickness. From Fig. S2b one can see that ζ increases linearly with thermal conductivity of the substrate, because ΔT is inversely proportional to κ_s (see (S9)). Interestingly, in the considered frequency range, δT does not depend on R , κ_l , c_s , as well, and depends only on c_f . Thus, the parameter ζ is controlled by Eq. (S9). Hence, in the case of a Si substrate, the efficiency can be more than two times larger than for GaAs, due to the difference in their heat conductivities. The dependence of the dynamical harvesting efficiency on c_f is shown in Fig. 2c. Thus, the efficiency can be larger than in Galfenol for materials with smaller c_f .

Finally, we discuss the design of a device with a ferromagnetic harvester, which uses the heat generated in a conducting layer in the vicinity of the harvester (see Fig. S3). Consider a thin conducting layer (e.g., a quantum well or a graphene layer) with thickness, l , which is separated from the harvester by a spacer with thickness, s . The harvester's thickness is h . We calculate ζ for such a device using an approach similar to that described in the Supplementary Notes 1 and 2. In our example, we take $h = l = 5$ nm, and $s = 2.5$ nm. For the conducting layer, spacer and

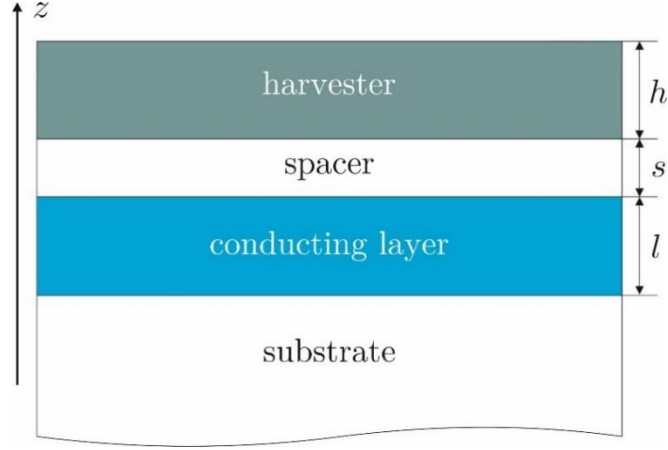


Fig. S3. Scheme of the device with a thin conducting layer and a ferromagnetic harvester.

substrate, we use the same thermal parameters as for GaAs. We consider that the heat is periodically released only in the conducting layer at $f_0 = 10$ GHz. In the real device the heat source may be Joule heat emitted as result of an electrical current injected on the clock frequency f_0 . For the harvester, we take Galfenol. In this case, the calculated efficiency $\zeta = 0.004$ which is only two times smaller than the efficiency of the system used in our experiments.

Note 4. Magnon dispersion

The frequency of thermally excited spin waves (magnons) in the studied Galfenol nanolayer is determined by the external magnetic field, \mathbf{B} , and the magnon wave vector, \mathbf{q} . The frequency of the ground magnon mode, which corresponds to the case of uniform precession ($q=0$), is given by the well-known expression [S2]:

$$f = \frac{\gamma_0}{2\pi} \sqrt{F_{\phi\phi} F_{\theta\theta}}, \quad (\text{S11})$$

where γ_0 is the gyromagnetic ratio, and $F_{\theta\theta} = \frac{\partial^2 F_M}{\partial \theta^2}$ and $F_{\phi\phi} = \frac{\partial^2 F_M}{\partial \phi^2}$ are the second derivatives of the free energy density (see Eq.2 in the main text) with respect to the in-plane azimuthal angle, ϕ , and polar angle, θ , calculated at the equilibrium orientation of magnetization. The angles are counted from the [100] crystallographic direction and from the normal to the layer plane, respectively. Using the free energy density as in Ref. [3] and considering the case of an in-plane external magnetic field we get:

$$F_{\theta\theta} = B \cos(\phi_M - \phi_B) + \mu_0 M_0 + \frac{K_1}{2} (\cos 4\phi_M + 3) + K_u (1 + \sin 2\phi_M) \quad (\text{S12})$$

$$F_{\phi\phi} = B \cos(\phi_M - \phi_B) + 2K_1 \cos 4\phi_M + 2K_u \sin 2\phi_M$$

where K_1 , K_u and M_0 are the temperature dependent cubic and uniaxial anisotropy coefficients, and the saturation magnetization, respectively; ϕ_b is the in-plane angle of the external magnetic field and ϕ_M is the field-dependent angle of the equilibrium orientation of magnetization (at $B > 0.3T$, $\phi_M = \phi_b$). In the experimental temperature range the temperature dependences of K_1 , K_u and M_0 may be written as: $X = X^{RT} + \beta_X (T - T_0)$, where $X = K_1, K_u$ or M_0 [S4]; X^{RT} are their values at room temperature and $\beta_X = \frac{\partial X}{\partial T}$ is the temperature independent coefficient. The dependences $f(B)$ calculated for $\phi_b = -\pi/8$ for room temperature and $\Delta T = 200$ K are shown in Fig.

1a of the main text. The parameters used for the calculations are the following [S3,S4]: $M_0^{RT} = 1.95 \text{ T}$, $K_1^{RT} = 20 \text{ mT}$, $K_u^{RT} = 9 \text{ mT}$, $\beta_M = -0.97 \text{ mT/K}$, $\beta_{K1} = -0.046 \text{ mT/K}$, $\beta_{Ku} = -0.025 \text{ mT/K}$.

Due to the finite laser spot size, the thermal modulation generates also magnons with non-zero in-plane wave vectors, q_{\parallel} . The range of in-plane wave vectors is set by the laser spot. It is found from the Fourier transform of the Gaussian distribution of the laser intensity (see Eq. (S7)). Therefore, we obtain $0 \leq q_{\parallel} \leq \frac{4}{r}$, where r is the laser spot radius. In our experiment with $r = 8.5 \text{ }\mu\text{m}$ the upper limit is $q_{\parallel} \leq 4700 \text{ cm}^{-1}$. This range corresponds to magneto-static spin waves with a very weak dispersion determined by the magnetic dipole-dipole interaction. This dispersion is strongest for the wave vectors perpendicular to the external magnetic field [S5]. In the case of a thin ferromagnetic film of thickness, h , where $\frac{q_{\parallel}h}{2\pi} \ll 1$ it can be written in a simplified form as [S6]:

$$f_{q_{\parallel}} = f + \frac{\gamma_0}{2\pi} \nu q_{\parallel} h, \quad (\text{S13})$$

where ν is the dispersion coefficient determined by the main parameters of the ferromagnet: K_1 , K_u and M_0 . For the studied Galfenol layer its value at room temperature is $\nu \approx 3.8 \text{ T}$ [S7] and in our experiment the frequencies of the thermally driven magnons with finite in-plane wave vector do not exceed 270 MHz. This value is less than the spectral width of the fundamental magnon mode (0.5 GHz) determined by the precession decay. Thus, the thermally driven magnons with finite in-plane wave vectors may be considered as degenerate.

The spectrum of magnons with finite tangential wave vector, q_{\perp} , is quantized due to spatial confinement along the layer normal: $q_{\perp,n} = \frac{\pi n}{h}$, where $n=1,2,3\dots$. In layers with nanometer thickness, the corresponding dispersion is determined by the exchange interaction and in a simplified form can be written as:

$$f_n = f + \frac{\gamma_0}{2\pi} \rho D q_{\perp,n}^2, \quad (\text{S14})$$

where D is the spin stiffness constant and ρ is a field dependent coefficient approaching 1 with increasing B [S8]. In the studied Galfenol layer with $h=5 \text{ nm}$, the large penetration depth of the laser pulse in comparison with the layer thickness results in uniform thermal distribution along the layer normal. Thus, the odd magnon modes ($n=1,3,5$) cannot be excited. The lowest higher-order mode, which can be driven by thermal modulation, corresponds to $n=2$. For the Galfenol spin stiffness $D=1.5 \times 10^{-17} \text{ Tm}^2$ [S8, S9], the frequency of this mode exceeds the ground mode frequency by more than 500 GHz. Due to the extremely low amplitude of such high-frequency harmonics in the thermal spectrum, this mode as well as other higher-order even modes are not excited. Thus, in the studied layer of 5-nm thickness the fundamental magnon mode is solely driven by the modulated heat.

The situation changes drastically in a ferromagnetic layer with thickness $\sim 100 \text{ nm}$, which possesses significantly less spectral splitting of the higher-order magnon modes with finite q_{\perp} . Due to the small penetration depth of light in comparison with the layer thickness, both odd and even modes can be excited [S8,S10]. This results in a drastic broadening of the magnon spectrum and a corresponding dephasing of the magnetization precession with destructive effects on the resonant energy harvesting. This is clearly seen in Fig. S4, which summarizes the experimental results obtained for a Galfenol layer of thickness $h=105 \text{ nm}$. The upper inset shows the magnon

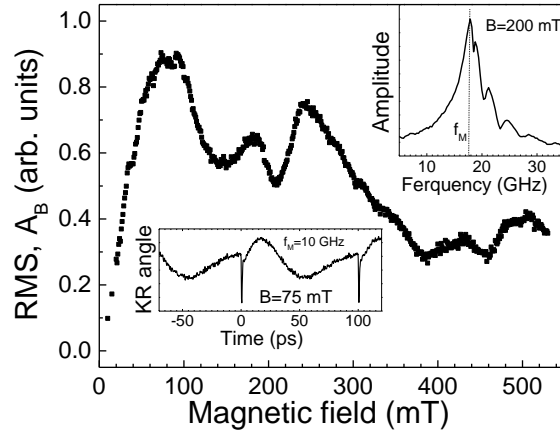


Fig. S4. Magnetic field dependences of the root mean square (RMS) Kerr rotation amplitude, \widetilde{A}_B , measured in a Galfenol layer of 105-nm thickness for the excitation power $W=140$ mW. The upper inset shows the magnon spectrum obtained as the fast Fourier transform of the Kerr rotation signal measured in a single pulse pump-probe experiment at $B=200$ mT. The lower inset shows the transient Kerr rotation signal measured for 10-GHz optical excitation at $B=75$ mT

spectrum obtained by fast Fourier transforming the Kerr rotation signal measured in a single pulse pump-probe experiment at $B=200$ mT. In addition to the dominating fundamental magnon mode, the FFT includes several spectral lines, which correspond to the higher-order magnon modes with $n=1\dots5$. Their spectral splitting is described with high accuracy by the dispersion relation [S7]. The result of such a spectral broadening becomes apparent in the transient KR signal measured under resonant conditions when $f=f_0=10$ GHz (see the lower inset). The non-harmonic character of the thermally driven oscillations in the KR signal is clearly seen. As a result, the field dependence of the RMS Kerr amplitude shown in the main panel consists of several broad peaks instead of narrow resonances as observed in the 5-nm Galfenol layer. At $B=75$ mT, which corresponds to the maximum amplitude of precession, its absolute values and RMS are 15-times smaller than in the 5-nm layer.

References

- [S1] COMSOL Multiphysics® v. 5.4. <http://www.comsol.com>. COMSOL AB, Stockholm, Sweden.
- [S2] Gurevich, A.G. & Melkov, G.A., Magnetization oscillations and waves (CRC-Press, Boca Raton, 1996).
- [S3] Kats, V. N. et al., Ultrafast changes of magnetic anisotropy driven by laser-generated coherent and noncoherent phonons in metallic films, *Phys. Rev. B* **93**, 214422 (2016).
- [S4] Clark, A. E. et al., Temperature dependence of the magnetic anisotropy and magnetostriction of $\text{Fe}_{100-x}\text{Ga}_x$ ($x=8.6, 16.6, 28.5$). *J. of Appl. Phys.* **97**, 10M316 (2005).
- [S5] Damon, R. W. & ESHBACH J. R., *J. Phys. Chem. Solids* **19**, 308-320 (1961).
- [S6] Kamimaki, A., Iihama, S., Sasaki, Y., Ando, Y., & Mizukami, S. Reciprocal excitation of propagating spin waves by a laser pulse and their reciprocal mapping in magnetic metal films. *Phys. Rev. B* **96**, 014438 (2017).
- [S7] Khokhlov, N. E. et al., Optical excitation of propagating magnetostatic waves in an epitaxial galfenol film by ultrafast magnetic anisotropy change. *Phys. Rev. Appl.* **12**, 044044 (2019).
- [S8] Scherbakov, A.V. et al., Optical excitation of single- and multimode magnetization precession in Fe-Ga nanolayers. *Phys. Rev. Appl.* **11**, 031003 (2019).
- [S9] Gopman, D. B., Sampath, V., Ahmad, B. H., Bandyopadhyay, S., & Atulasimha, J., Static and dynamic magnetic properties of sputtered Fe-Ga thin films, *IEEE Trans Magn.* **53**, 6101304 (2017).
- [S10] van Kampen, M. et al., All-optical probe of coherent spin waves. *Phys. Rev. Lett.* **88**, 227201 (2002).